


RESEARCH ARTICLE

Open Access



How large peak ground acceleration by large earthquakes could generate turbidity currents along the slope of northern Japan Trench

Ken Ikehara^{1*} , Kazuko Usami^{2,3} and Toshiya Kanamatsu⁴

Abstract

Deep-sea turbidite has been used to determine the history of occurrence of large earthquakes. Surface-sediment remobilization is a mechanism of the generation of earthquake-induced turbidity currents. However, the detailed mechanism of surface-sediment remobilization caused by earthquake ground shaking is unclear. To understand how high peak ground acceleration (PGA) caused by a large earthquake can remobilize surface sediments, we determined the age of a surface-sediment core recovered from the mid-slope terrace (MST) of the inner slope of the Japan Trench in northern Sanriku to determine turbidites generated by large historical earthquakes and calculate the PGAs of these earthquakes using an empirical attenuation relation commonly used in Japan. Small offsets in radiocarbon ages and excess ²¹⁰Pb activities between turbidite and hemipelagic muds suggest that the turbidites in the core resulted from surface-sediment remobilization. ¹³⁷Cs and excess ²¹⁰Pb chronologies indicate that the three uppermost turbidites in the core are correlated with three large historical earthquakes, namely the 1968 common era (CE) Tokachi-oki, the 1933 CE Showa–Sanriku, and the 1896 CE Meiji–Sanriku earthquakes. Calculation of PGAs for large historical earthquakes along the northern Japan Trench indicates that a PGA of > 0.6 g is necessary for turbidite deposition in the MST basin. This threshold is larger than that reported for central Sanriku and may vary spatially. Moreover, turbidites in the MST deposits are more frequent in the northern Japan Trench than in the central Japan Trench, suggesting that the occurrence of three types of large M8-class earthquakes in the northern Japan Trench might have contributed to the frequent occurrence of large PGAs.

Keywords Paleoseismology, Historical earthquake, Peak ground acceleration, Turbidite, Japan Trench

1 Introduction

Deep-sea turbidite has been used to determine the history of occurrence of large earthquakes (e.g., Adams 1990; Goldfinger et al. 2007, 2012; Patton et al. 2015; Ikehara et al. 2016). Large earthquakes are one of the main mechanisms of the initiation of turbidity currents, although other mechanisms have been proposed, such as storm surges, large storm waves, floods (hyperpycnal flows), rapid sediment loading, submarine groundwater discharge, volcanic eruption, and bolide impacts (e.g., Goldfinger et al. 2012; Pickering and Hiscott 2015). While earthquake-induced submarine landslides and transformation from landslides to turbidity currents through subaqueous debris flows, as exemplified by the

*Correspondence:

Ken Ikehara
k-ikehara@aist.go.jp

¹ Geological Survey of Japan, National Institute of Advanced Industrial Science and Technology (AIST), Tsukuba Central 7, 1-1-1 Higashi, Tsukuba, Ibaraki 305-8567, Japan

² Japan NUS Co. Ltd., Nishi-Shinjuku Prime Square 5F, 7-5-25

Nishi-Shinjuku, Shinjuku-Ku, Tokyo 160-0023, Japan

³ Japan Organization for Metals and Energy Security (JOGMEC), 1-2-2, Hamada, Mihama-Ku, Chiba 261-0025, Japan

⁴ Research Institute of Marine Geodynamics, Japan Agency for Marine-Earth Science and Technology (JAMSTEC), 2-15 Natsushima-Cho, Yokosuka, Kanagawa 237-0046, Japan

1929 common era (CE) Grand Banks earthquake, north-west Atlantic (Heezen and Ewing 1952; Heezen et al. 1954; Piper et al. 1999), are a major mechanism for generating earthquake-induced turbidites, another mechanism has recently been proposed. This involves the surface-sediment resuspension and remobilization caused by large ground shaking during large earthquakes (Moernaut et al. 2017). The obtained remobilization depths in the Chilean lakes range between 0.6 and 8.5 cm, with an average of 5.3 cm (Moernaut et al. 2017). The occurrence of turbidity currents of surface-sediment remobilization origin has been studied for several recent and historical large earthquakes (Moernaut et al. 2014, 2017; McHugh et al. 2016; Molenaar et al. 2019, 2021; Ikehara et al. 2020, 2021; Schwestermann et al. 2021). However, there is little knowledge on how large earthquake ground shaking causes surface-sediment remobilization. Although several papers have discussed the minimum peak ground acceleration (PGA) caused by large earthquakes that is needed to generate slope instabilities and turbidite depositions (e.g., Lee et al. 1999; Lykousis et al. 2002; Strasser et al. 2007; Noda et al. 2008; Dan et al. 2009; Pouderoux et al. 2014; Usami et al. 2018), the responses of slope sediments to earthquake ground shaking are spatially different, reflecting variations in topography (e.g., slope angle and roughness) and sedimentology (e.g., sediment thickness and grain size and composition). Therefore, it is crucial to gather examples of surface-sediment remobilization generated by historical earthquakes and understand the minimum PGA caused by large earthquakes that are necessary for initiation of turbidity currents from surface-sediment remobilization.

The mid-slope terrace (MST) is a deep-sea terrace with a water depth of 4000–6000 m; it is formed along a series of faults at the front of the backstop of the subducting Pacific Plate along the central to northern Japan Trench (von Huene et al. 1980; Tsuru et al. 2002). Sediments supplied by gravity flows from the landward slopes are trapped at this flat terrace (von Huene and Culotta 1989; Tsuru et al. 2002; Usami et al. 2018; Ikehara et al. 2020). Gravity flows by surface-sediment remobilization is a mechanism of earthquake-induced downslope sediment transport along the MST (McHugh et al. 2016; Molenaar et al. 2019; Ikehara et al. 2020, 2021). Turbidites generated by recent and historical earthquakes were reported from the central MST (McHugh et al. 2016; Usami et al. 2018). Therefore, the MST along the Japan Trench is an ideal area for examining the threshold of PGA caused by large historical earthquakes that are needed to create turbidity currents via surface-sediment remobilization.

In this paper, we examine a surface-sediment core collected from the northern MST, where recent and historical earthquakes have occurred in different patterns from

the central MST, to determine turbidites formed by large historical earthquakes. We discuss the minimum PGA needed to generate surface-sediment remobilization along the slope.

2 Material and methods

2.1 The mid-slope terrace along the northern Japan Trench and surface-sediment core

At the Japan Trench, the Pacific Plate subducts north-westward the Okhotsk Plate at a rate of 8.0–8.6 cm/year (DeMets et al. 2010). The continuous fault activity along the Japan Trench produces a backstop interface and the MST has been formed along the faults at the backstop (von Huene et al. 1980; Tsuru et al. 2002). The sediments transported by gravity flows from the inner (landward) slope are trapped in a series of isolated depressions of the MST with little lateral migration of sediments (von Huene and Culotta 1989; Tsuru et al. 2002; Usami et al. 2018; Ikehara et al. 2020). The lack of submarine canyon connecting the shelf and the MST off the Sanriku slope suggests that storm- and flood-related turbidity currents can hardly reach the MST and earthquakes are the most likely mechanism of the generation of the turbidity currents on this slope.

The sediments at the MST are generally diatomaceous (Mann and Müller 1980; Usami et al. 2018; Ikehara et al. 2020, 2021), reflecting high diatom productivity in the surface water (Saino et al. 1998). High average sedimentation rates are observed at the MST (100–110 cm/ky), and the MST deposits comprise the alternation of bioturbated hemipelagic muds and muddy turbidites (Usami et al. 2018; Ikehara et al. 2020). Several large ($M > 7.6$) and recent earthquakes have occurred around the central–northern Japan Trench (Tajima et al. 2013; Satake 2015; Toda 2016; Lay 2018; Headquarters for Earthquake Research Promotion 2019). These were the 2011 CE off the Pacific coast of Tohoku earthquake (Tohoku-oki; M 9.0, M_w 9.1), 1994 CE Sanriku-oki earthquake (M 7.6, M_w 7.8), 1968 CE Tokachi-oki earthquake (M 7.9, M_w 8.2), 1933 CE Sanriku-oki outer-rise earthquake (Showa–Sanriku; M 8.3, M_w 8.4), 1931 CE Sanriku-oki earthquake (M 7.6, M_w 7.8), and 1896 CE Sanriku-oki tsunami earthquake (Meiji–Sanriku; M 8.1, $M_w \sim 8.1$) (M_w values from Lay 2018). Large recent and historical earthquakes have caused turbidite deposition in the MST depressions and downslope sediment transport (McHugh et al. 2016; Usami et al. 2018; Molenaar et al. 2019).

We obtained core YK14-E01 PL08 (location: N 40°08.0264', E 143°57.9590'; water depth: 4203 m; core length: 95 cm) from a small basin at the MST off Kuji, northern Sanriku, using a gravity corer during the YK14-E01 cruise of R/V Yokosuka (Fig. 1; <http://www.jamstec.go.jp/datadoi/doi/10.17596/0001654.html>). Because the

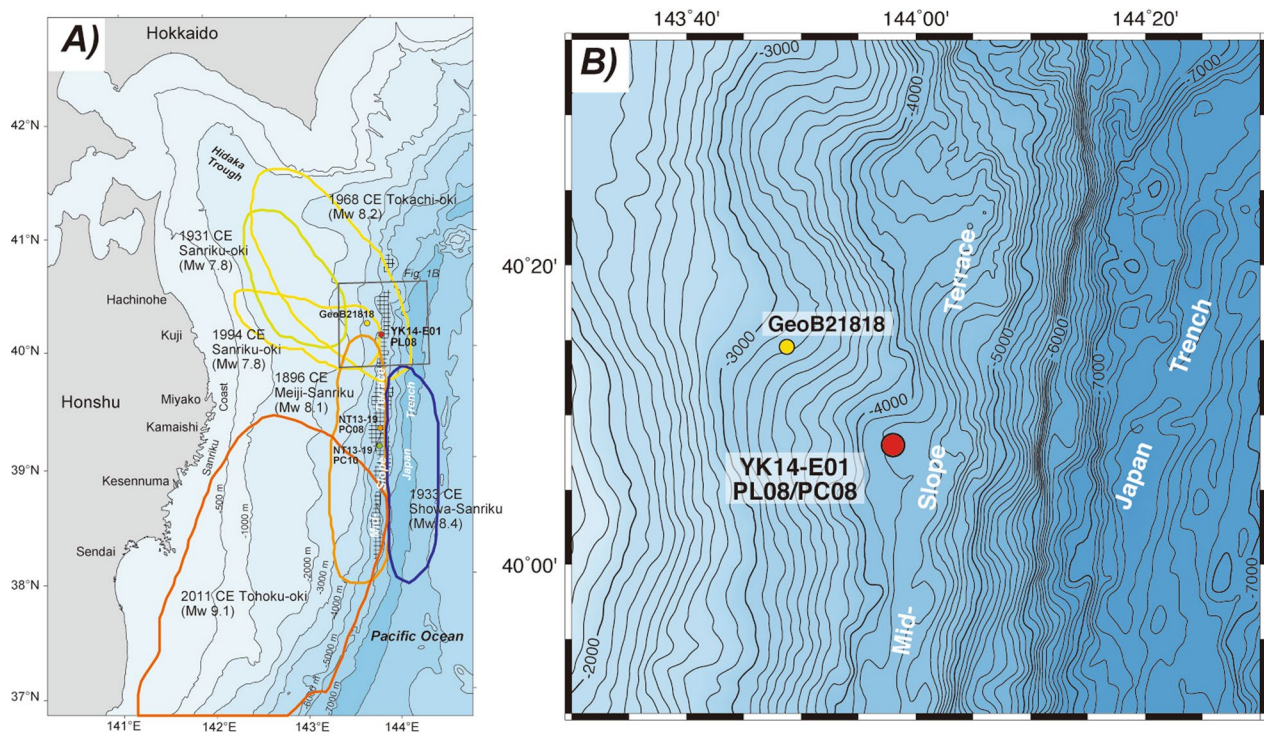


Fig. 1 Bathymetry and location of the studied coring site (solid red circle: YK14-E01 PL08). **A** Rupture zones of large historical earthquakes. The hatched area is the MST. The three coring sites are shown. Solid orange circle: NT13-19 PC08, solid green circle: PC10, and solid yellow circle: GeoB21818. **B** Detailed bathymetry around the studied coring site (solid red circle) and slope coring site (solid yellow circle: GeoB21818)

gravity corer was used as a trigger of a piston corer, free fall was not used, and an undisturbed sample of the sediment–water interface was obtained. The coring site was at the same location as the piston core (YK14-E01 PC08), which was used by Ikehara et al. (2020).

2.2 Determination of event deposits

The core was cut vertically, and the sedimentary structures, sediment color, grain size, and grain composition on the cut surface of one-half were logged visually. X-radiographs of 1 cm thick slab samples were obtained at the Geological Survey of Japan, AIST, to observe their detailed sedimentary structures and radiodensity. Magnetic properties, such as mean magnetic susceptibility (K), magnetic lineation (L), and magnetic foliation (F), were measured using continuously collected standard paleomagnetic plastic cube samples (7 cm³) and a KLY-4 magnetic susceptibility meter (Agico Co.) at JAMSTEC. A total of 78 discrete samples were analyzed: 41 from core PL08 and 37 from the uppermost Sect. (85.5 cm in length) of core PC08. The mean magnetic susceptibility and two magnetic fabric parameters (lineation and foliation) were obtained from three eigenvectors, namely, K_1 , K_2 , and K_3 , which are the maximum-, intermediate-, and

minimum-susceptibility axes, respectively (Hrouda 1982; Tarling and Hrouda 1993).

$K = (K_1 + K_2 + K_3) / 3$ (mean susceptibility; Nagata 1961).

$L = K_1 / K_2$ (magnetic lineation; Balsley and Buddington 1960).

$F = K_2 / K_3$ (magnetic foliation; Stacey et al. 1960).

The horizons of muddy turbidites were determined using a combination of sedimentary and magnetic signatures. Small offsets in radiocarbon ages between the turbidite muds and the underlying or overlying hemipelagic muds are useful for studying the surface-sediment remobilization of turbidite origin (Okutsu et al. 2019; Ikehara et al. 2020). The radiocarbon ages of five turbidite mud samples and five hemipelagic mud samples were determined using bulk organic carbon in sediments to determine the age offset between the two sample groups. The bulk sediment samples used for measurement, sized 5–10 cm³, were washed with acid to remove carbonates prior to measurement. The stable carbon isotope ratios ($\delta^{13}\text{C}$) of the same samples for radiocarbon dating were determined using an isotope-ratio mass spectrometer. The radiocarbon dates and stable carbon isotopes were measured in the accelerator mass spectrometer radiocarbon facility at Beta Analytics Co. Ltd.

2.3 Age determination

Radioactivity for ^{137}Cs , ^{210}Pb , and ^{214}Pb in 20 sediment samples of 8–18 g in wet weights was measured at 1–2 cm intervals by Environchron Inc. at Eckerd College Marine Science Department (Florida). The samples were ground to fine powder, weighed, and sealed in a 4 cm diameter counting container. We used a Mirion (Canberra) high-purity germanium coaxial planar photon detector linked to a multichannel analyzer (Mirion (Canberra) DSA 1000), and the measurement time was ~24–50 h. Data were corrected for emission probability at the measured energy, counting time, and sample mass and then converted to activity (disintegrations per gram, dpm/g) using the International Atomic Energy Association (IAEA) organic standard IAEA-477 for calibration (Kitto 1991; Larson et al. 2018). Excess ^{210}Pb was defined as the difference between the measured activities (dpm/g) of supported and unsupported ^{210}Pb and supported ^{210}Pb , which was determined by averaging the activity of its parent radioisotopes, ^{214}Pb and ^{214}Bi , assuming the uranium series had reached secular equilibrium (Kato et al. 2003). The excess ^{210}Pb -derived age model was calculated using a constant initial concentration model assuming constant excess ^{210}Pb concentration upon sedimentation (Cundy and Croudace 1995; Kanai 2000). The ^{137}Cs activity profile (peak and first occurrence of ^{137}Cs activity) was used to determine the start of atmospheric nuclear bomb experiments, which were detected in 1955 CE, and the peak of ^{137}Cs fall-out in 1963 CE in Japan (Hirose et al. 1987, 2008; Igarashi et al. 1996). For the correlation of turbidites in cores PL08 and PC08 (Ikehara et al. 2020), which were obtained from the same location, excess ^{210}Pb and ^{137}Cs activities were also measured for nine samples of hemipelagic muds from the upper part of core PC08.

The radiocarbon ages of bulk organic carbon in hemipelagic muds are important for sediment age determination in the environment below the calcium carbonate compensation depth. However, previous study (e.g., Ikehara et al. 2020) has reported that there is a larger uncertainty in the depositional ages estimated from the radiocarbon ages than those estimated from ^{137}Cs and excess ^{210}Pb chronology. Therefore, herein, we used the radiocarbon ages of bulk organic carbon only for discussing the age offset between hemipelagic and turbidite muds and not for sediment age determination.

2.4 Estimation of PGA

We estimated the maximum acceleration caused by historical earthquakes on the inner slope of the coring site. Six large historical earthquakes that occurred around the coring sites were selected for calculation: the 2011

CE Tohoku-oki, 1994 CE Sanriku-oki, 1968 CE Tokachi-oki, 1933 CE Showa–Sanriku, 1931 CE Sanriku-oki and 1896 CE Meiji–Sanriku earthquakes. Several methods have been proposed for PGA calculation (e.g., Fukushima and Tanaka 1990; Zhao et al. 1997; Si and Midorikawa 1999). We used an empirical attenuation relation that is commonly used in Japan and derived from records of ground motion on land (Si and Midorikawa 1999) and is the same as that proposed by Usami et al. (2018), who examined the PGA for turbidite depositions at the central MST, because we would like to discuss the spatial variability of PGA along the slope of the Japan Trench.

$$\text{Log (PGA)} = b - \log(x + c) - 0.003x, \quad (1)$$

where

$$b = 0.5M_w + 0.0043D + d + 0.61, \quad (2)$$

$$c = 0.0055 * 10^{0.50M_w}, \quad (3)$$

where x is the shortest distance from the fault plane (fault distance), D is the focal depth (average depth of the fault plane), and d corresponds to the type of earthquake (crustal: 0.00; interplate: 0.01; intraplate: 0.22). We applied $d=0.01$ in the calculations because the studied earthquakes were all interplate earthquakes except for the 1933 CE Showa–Sanriku earthquake, which was an outer-rise earthquake within the subducting plate. However, we used the same d value for the 1933 CE Showa–Sanriku earthquake in this calculation. We calculated PGA at an assumed source point of sediments at the landward slope near our coring site, namely the GeoB21818 coring site (N 40°14.790, E 143°48.918'), which was on a slope at a 3139 m water depth (the location shown in Fig. 1B), where sedimentation gaps caused by earthquake-induced surface-sediment remobilization were found in a surface-sediment core sample (Moleenaar et al. 2019). Focal depths of 24, 10, 10, and 7 km were used for the 2011 CE Tohoku-oki (Yoshida et al. 2011), 1994 CE Sanriku-oki (Nagai et al. 2001), 1933 CE Showa–Sanriku (Kanamori 1971), and 1896 CE Meiji–Sanriku earthquakes (Satake et al. 2017), respectively. For the 1968 CE Tokachi-oki and 1931 CE Sanriku-oki earthquakes, a focal depth of 10 km, which is the same depth as that of the 1994 CE Sanriku-oki earthquake, was set assuming all ruptured the same asperity (Nagai et al. 2001). Strong ground motion stops increasing with M_w for earthquakes with $M_w > 8.3$ (called magnitude saturation) when using fault distance for calculation (Si et al. 2016). For the 2011 CE Tohoku-oki earthquake, we used M_w 8.4 for calculation. Because this attenuation formula was developed from on land records and high-frequency seismic waveguides more efficiently in the subducting

Pacific Plate than in the overriding (landward) plate (Furumura and Kennett 2005), the actual PGAs in the deep-sea close to the Pacific Plate may be stronger.

3 Results and discussion

3.1 Sediment lithology and turbidite recognition

A total of six coarse-grained layers (T-L1–T-L6) consisting of a basal coarse-grained part and an overlying muddy part were identified in bioturbated diatomaceous muds (Fig. 2 and Table 1). Each coarse-grained layer is 1–3 cm in thickness and characterized by a sharp base and fining-upward grading (Fig. 2). Parallel- or cross-laminations are observed in some basal parts. A homogeneous structure without bioturbation is a characteristic feature of the upper part. These features suggest that the basal coarse-grained layers and overlying homogeneous muds are fine-grained turbidites (Stow and Shanmugam

1980). Turbidite muds and hemipelagic muds can be distinguished by the following characteristics: sedimentary structure, radiodensity (X-ray transparency), sediment color, and magnetic parameters (Fig. 2; Additional file 1: Table S1). Turbidite muds are originally homogeneous in structure and olive black in color and show an increase in radiodensity, mean magnetic susceptibility ($> \sim 0.0004$ SI), and magnetic foliation ($> \sim 1.02$), although they are occasionally disturbed by post-depositional burrowing. By contrast, hemipelagic muds are completely bioturbated, have lower radiodensities, are gray–grayish olive–olive black in color, and have lower mean magnetic susceptibility ($< \sim 0.0004$ SI) and magnetic foliation ($< \sim 1.04$). Magnetic lineation in turbidite muds is slightly higher ($> \sim 1.01$) than that in hemipelagic muds ($< \sim 1.01$). High magnetic foliation in turbidite muds, which has been reported in muddy turbidites or homogenites in

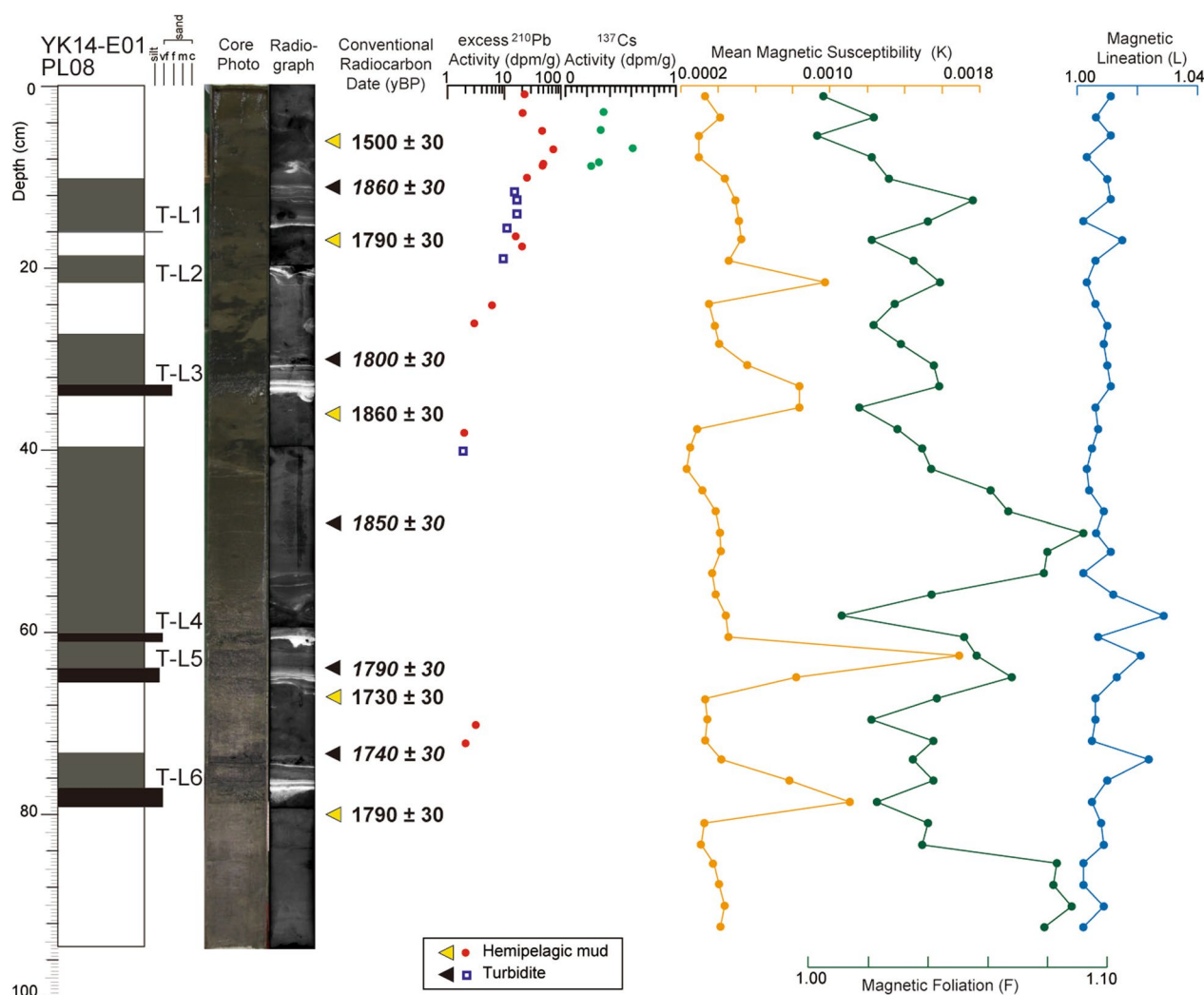


Fig. 2 Sedimentological, magnetic, and chronological characteristics of core YK14-E01 PL08

Table 1 Turbidites in core YK14-E01 PL08

Turbidite No	Top depth (cm)	Bottom depth (cm)	Thickness (cm)	Thickness of basal coarse part (cm)	Sedimentary structures
T-L1	10.0	16.0	6.0	1.0	Parallel-/ripple-laminated, sharp base
T-L2	18.5	21.6	3.1	1.6	Parallel-laminated, partly disturbed by post-depositional burrow, sharp base
T-L3	27.2	34.0	6.8	1.2	Parallel-/cross-laminated, graded, sharp base
T-L4	39.6	61.0	21.4	1.0	Parallel-/cross-laminated, graded, sharp base
T-L5	61.0	65.7	4.7	1.7	Parallel-laminated, graded, sharp base
T-L6	73.2	79.2	6.0	2.2	Parallel-/cross-laminated, graded, sharp base

marine settings (Abdeldayam et al. 2004; Campos et al. 2013) and lacustrine settings (Beck 2009; Petersen et al. 2014), results from oscillations in water mass during the slow deposition of resuspended fine particles (Beck 2009; Campos et al. 2013). Kase et al. (2016) studied the characteristic occurrence of aggregates of clay particles, which may be formed by the collision of flocs in turbulent flows, in turbidite mud. Original edge-to-face clay contact patterns of the flocs were preserved in the aggregates, whereas the flocs were broken after deposition, and a randomly oriented structure was formed in hemipelagic muds (Kase et al. 2016). Such differences in clay fabric between turbidite and hemipelagic muds may result in higher magnetic foliation in turbidite muds than in hemipelagic muds. Although the origin of high magnetic foliation remains unclear, magnetic foliation is a useful proxy for differentiating turbidite and hemipelagic muds.

3.2 Surface-sediment remobilization as revealed by offset of radiocarbon ages and excess ^{210}Pb activities between turbidite and hemipelagic muds

The offsets in radiocarbon ages between the turbidite muds and the underlying or overlying hemipelagic muds in core PL08 are small (−50–120 years; Table 2) and

close to those in core PC08 (−40–330 years except for two turbidites; Ikehara et al. 2020), where most turbidites in core PC08 are the results of surface-sediment remobilization (Ikehara et al. 2020). The offsets in excess ^{210}Pb activities between the turbidite and hemipelagic muds in core PL08 are also small (Fig. 2).

Age offset between the 2011 CE Tohoku-oki earthquake turbidite and the underlying hemipelagic muds is small in a central Japan Trench basin (Bao et al. 2018). The 2011 CE turbidites in the nearby central Japan Trench basins at ~N 38° contain ^{137}Cs and excess ^{210}Pb (Oguri et al. 2013; Ikehara et al. 2016) and fresh organic matter (Schwestermann et al. 2021). Thus, the small age offset between the turbidite and hemipelagic muds suggests little mixture of old organic matter from deep subsurface sediments in the turbidite muds and is considered a proxy for surface-sediment remobilization (Okutsu et al. 2019; Ikehara et al. 2020). The small offsets in excess ^{210}Pb activities suggest that origin of turbidite muds is the young surface sediments containing similar activities to the hemipelagic muds. High activities of excess ^{210}Pb were identified in the event deposits formed by the 2011 CE Tohoku-oki earthquake and its associated tsunami (Ikehara et al. 2021).

Table 2 Radiocarbon ages and age offsets between turbidite muds and hemipelagic muds

	Sample ID	Sample depth (cm)	Conventional ^{14}C age	$\delta^{13}\text{C}$	Turbidite no	Age offset	Accession no
1	YK14L0806H	6–8	1500 ± 30	−20.45			Beta-632753
2	YK14L0811T	11–13	1860 ± 30	−20.77	T-L1	70 (2–3)	Beta-632754
3	YK14L0817H	17–19	1790 ± 30	−20.10			Beta-632755
4	YK14L0830T	30–32	1800 ± 30	−20.24	T-L3	−60 (4–5)	Beta-632756
5	YK14L0838H	38–40	1860 ± 30	−19.97			Beta-632757
6	YK14L0848T	48–50	1850 ± 30	−19.95	T-L4	120 (6–8)	Beta-632758
7	YK14L0862T	62–64	1790 ± 30	−20.19	T-L5	60 (7–8)	Beta-632759
8	YK14L0867H	67–69	1730 ± 30	−20.57			Beta-632760
9	YK14L0873T	73–75	1740 ± 30	−20.01	T-L6	−50 (9–10)	Beta-632761
10	YK14L0880H	80–82	1790 ± 30	−20.10			Beta-632762

The stable carbon isotope ratios ($\delta^{13}\text{C}$) of bulk organic carbon range from -19.95 to -20.77 ‰ (-19.95 to -20.77 ‰ for the turbidite muds and -19.97 to -20.57 ‰ for the hemipelagic muds; Table 2). The lack of a significant difference in the $\delta^{13}\text{C}$ values between the turbidite and hemipelagic muds in core PL08 suggests a deep-marine source of the turbidite muds. Therefore, offshore marine surface sediments are the most likely source of turbidite muds.

Although massive tsunamis are possible trigger mechanisms to transport shallow marine and coastal sediments to deep sea (Arai et al. 2013; Ikehara et al. 2021), the $\delta^{13}\text{C}$ values suggest that the tsunamis are not likely the mechanism for the formation of the turbidites in this core.

3.3 Excess ^{210}Pb and ^{137}Cs age model and correlation of turbidites with historical earthquakes

A peak of ^{137}Cs activity (0.61 dpm/g) occurs at a depth of 7 cm just above the uppermost turbidite (T-L1; Fig. 2 and Table 3). ^{137}Cs activity is not detected below 10 cm from the core top. The absence of ^{137}Cs below T-L1 and its stable detection above T-L1 suggest that T-L1 was formed near the peak fall-out of ^{137}Cs around the Japanese islands in 1963 CE (Hirose et al. 1987, 2008; Igarashi et al. 1996). Excess ^{210}Pb activities are low in the uppermost 3 cm (~ 20 dpm/g) and peak at a depth of 7 cm (73.55 dpm/g); they decrease toward a depth of 26 cm (2.98 dpm/g) and then fall below the detection limit ($< \sim 2$ dpm/g) at depths deeper than 38 cm (Fig. 2 and Table 3). Assuming the core top 2014 CE and a linear relationship between excess ^{210}Pb activities and the turbidite-free core depths of the hemipelagic muds, which is

Table 3 Results of radioactivity measurement

Core	Depth (top) (cm)	Depth (bottom) (cm)	Hemipelagic (H)/ Turbidite (T)	Horizon	ex ^{210}Pb (dpm/g)	Error	Depositional age (CE)	^{137}Cs (dpm/g)	Error
1 YK14-E01 PL08	0.0	2.0	H	Above T-L1	22.31	0.85	1945	ND	
2	2.0	4.0	H	Above T-L1	20.19	0.72	1942	ND	
3	2.0	4.0	H	Above T-L1	21.62	0.82	1944	0.35	0.07
4	4.0	6.0	H	Above T-L1	46.71	1.03	1969	0.32	0.06
5	6.0	8.0	H	Above T-L1	73.55	1.32	1983	0.61	0.09
6	8.0	9.0	H	Above T-L1	48.89	0.98	1970	0.30	0.06
7	8.0	10.0	H	Above T-L1	48.37	1.16	1970	0.24	0.06
8	9.0	11.0	H	Above T-L1	24.70	0.71	1948	ND	
9	11.0	12.0	T	T-L1	14.72	0.75	1931	ND	
10	12.0	13.0	T	T-L1	16.74	0.86	1936	ND	
11	13.0	15.0	T	T-L1	16.54	0.63	1935	ND	
12	15.0	16.0	T	T-L1	1112	0.41	1922	ND	
13	16.0	17.0	H	T-L1-T-L2	15.77	0.82	1934	ND	
14	17.0	18.0	H	T-L1-T-L2	20.13	0.68	1942	ND	
15	18.0	20.0	T	T-L2	9.70	0.49	1918	ND	
16	23.0	25.0	H	T-L2-T-L3	5.92	0.53	1902	ND	
17	25.0	27.0	H	T-L2-T-L3	2.98	0.37	1880	ND	
18	37.0	39.0	H	T-L3-T-L4	1.94	0.38	1866	ND	
19	39.0	41.0	T	T-L4	1.82	0.24	1864	ND	
20	69.0	71.0	H	T-L4-T-L5	3.14	0.36	1882	ND	
21	71.0	73.0	H	T-L4-T-L5	2.10	0.35	1869	ND	
22 YK14-E01 PC08	0.0	2.0	H	Above T1	23.37	0.94		0.23	0.06
23	2.0	4.0	H	Above T1	22.43	0.90		ND	
24	4.0	6.0	H	Above T1	52.82	1.44		ND	
25	6.0	8.0	H	Above T1	50.27	1.37		ND	
26	8.0	10.0	H	Above T1	70.54	1.61		ND	
27	30.0	32.0	H	T2-T3	7.16	0.36		ND	
28	32.0	34.0	H	T2-T3	4.46	0.47		0.17	0.05
29	43.0	43.0	H	T3-T4	2.72	0.41		ND	
30	45.0	47.0	H	T3-T4	2.36	0.37		ND	

established by removing the turbidites from the core, the depositional ages of each analyzed horizon are calculated from the constant initial accumulation model (Table 3).

Based on the estimated depositional ages from excess ^{210}Pb and ^{137}Cs activities, the three uppermost turbidites can be correlated with three historical earthquakes of the northern Japan Trench. The uppermost turbidite (T-L1) is just below the peak of ^{137}Cs activity, suggesting that it occurred around the 1960s CE, although the excess ^{210}Pb -based age model implies that T-L1 was deposited between 1948 and 1934 CE. The depositional ages of the second (T-L2) and third (T-L3) turbidites are between 1918 and 1902 CE and between 1880 and 1866 CE, respectively. Comparison with the recognized earthquakes in the northern Japan Trench region suggests that T-L1, T-L2, and T-L3 were most likely formed by the 1968 CE Tokachi-oki (Mw 8.2), 1933 CE Showa-Sanriku (Mw 8.4), and 1896 CE Meiji-Sanriku (Mw ~8.1) earthquakes, respectively. Slight older ages of the excess ^{210}Pb -based age estimation may afford relatively constant and low excess ^{210}Pb activities in the uppermost 3 cm of core PL08. Usami et al. (2018) reported that turbidites formed by the 1896 CE Meiji-Sanriku earthquake were just above the detection limit of excess ^{210}Pb in two cores off central Sanriku: NT13-19 PC08 (N 39°16.4448', E 143°56.6842') and NT13-19 PC10 (N 39°07.2353', E 143°54.1586'). According to Molenaar et al. (2019), the surface-sediment gap on the northern Japan Trench slope (core GeoB21818) resulted from the 1896 CE Meiji-Sanriku earthquake and was near the detection limit of excess ^{210}Pb . Thus, the event deposits from the 1896 CE Meiji-Sanriku earthquake are widely distributed more than 100 km along the northern-central Japan Trench slope and can be recognized using the profile of excess ^{210}Pb activity.

3.4 PGA threshold for initiation of earthquake-induced surface-sediment remobilization along the northern Japan Trench landward slope

Strong earthquake ground shaking is essential for earthquake-induced surface-sediment remobilization (Moernaut et al. 2014, 2017; Usami et al. 2018; Molenaar et al. 2019, 2021; Ikehara et al. 2021). Table 4 summarizes the PGAs at the assumed sediment source at the landward slope of our coring site caused by the studied historical earthquakes determined using the observed or estimated fault parameters. The PGA needed to form earthquake-induced turbidites at our coring site is approximately 0.6 g (Fig. 3). No turbidite is recognized by historical earthquakes of <0.6 g at the sediment source. Therefore, based on the examples of three historical earthquakes, the turbidites occurred in the studied MST basin are the

Table 4 Fault parameters and calculated PGA at an assumed sediment source point (GeoB21818 coring site) for six large recent and historical earthquakes

EQ	Mw	Focal depth (km)	Fault distance (km)	PGA (G)
2011 Tohoku-oki	9.1	24	67	0.35
1994 Sanriku-oki	7.8	10	14	0.59
1968 Tokachi-oki	8.2	10	14	0.64
1933 Showa-Sanriku	8.4	10	18	0.63
1931 Sanriku-oki	7.8	10	22	0.49
1896 Meiji-Sanriku	8.1	7	14	0.61

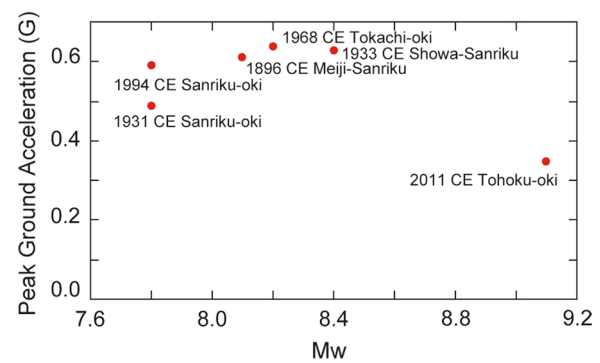


Fig. 3 PGA versus M_w for the six examined large earthquakes in the central-northern Japan Trench. PGA was calculated at an assumed sediment source point on the landward slope of our coring site (GeoB21818 coring site). Location of site GeoB21818 is shown in Fig. 1B

most likely record of past large earthquakes of > ~0.6 g at the source slope.

Based on the profile of excess ^{210}Pb activity of the surface sediments of core GeoB21818, which was collected updip of our coring site, Molenaar et al. (2019) stated that a few centimeters to 12 cm sediment remobilization occurred due to three large recent and historical earthquakes (2011 CE Tohoku-oki, 1968 CE Tokachi-oki, and 1896 CE Sanriku-oki earthquakes). However, we found no evidence of turbidite deposition by the 2011 CE Tohoku-oki earthquake, which has a PGA of 0.35 g, in core PL08. Instead, we found turbidite by the 1933 CE Showa-Sanriku earthquake, with a PGA of 0.63 g. Molenaar et al. (2019) proposed an earthquake-magnitude control rather than PGA control on surface-sediment remobilization. However, our turbidite results suggest clear PGA control (>0.6 g) for turbidite deposition in the northern MST sediments. Distance from the rupture area to the coring site influences the PGA magnitude and thus turbidite deposition. The small-scale and low-concentration nature of the turbidity current caused by

the 2011 CE Tohoku-oki earthquake might be a possible reason for the absence of the corresponding turbidites in the MST sediments despite the occurrence of small-scale (2 cm thick) surface-sediment remobilization on nearby slopes (Molenaar et al. 2019). Ikehara et al. (2012) reported a similar absence of turbidites after small-scale turbidity current events caused by the 1997 CE Izu-tohoku earthquake swarm in western Sagami Bay, which was observed at the deep-sea observatory (Iwase et al. 1997). Another possibility is the short-distance transport of resuspended and remobilized sediments due to small-scale turbidity currents. Ikehara et al. (2021) discussed such short-distance transport for homogeneous muddy event deposits formed by the 2011 CE Tohoku-oki earthquake on the unconfined slopes offshore of southern Sanriku and Sendai. There is no signature of surface-sediment remobilization by the 1933 CE Showa–Sanriku earthquake in the sediments of a nearby slope (Molenaar et al. 2019), which may suggest uneven resuspension of surface sediments on the slope by earthquake ground shaking reflecting spatial variabilities in sediment availability, geotechnical properties and compaction state of surface sediments and/or multiple turbidite sources in the MST sediments. According to Molenaar et al. (2021), the slopes of Chilean lakes have patchy, centimeter-scale gaps in sediments.

The six turbidites in the gravity core PL08 are likely correlated with the turbidites in the piston core PC08

(Ikehara et al. 2020) acquired in the same location, based on sediment lithology, the detection limit of excess ^{210}Pb , and profiles of magnetic parameters (Fig. 4; Additional file 1: Table S1). The detection limit of excess ^{210}Pb is below T-L3 in core PL08 and below T-3 in core PC08. Although the values of mean magnetic susceptibility differ between cores PL08 and PC08, the three uppermost turbidites in core PC08 (T1–T3) are correlated with those in core PL08 (T-L1–T-L3). A 26.1 cm thick amalgamated turbidite in core PL08 (T-L4–T-L5) and another turbidite (T-L6) might be correlated with the T4 and T5 turbidites in core PC08, according to their stratigraphic position. The thick nature of turbidite muds is common in both T-L4 and T4. The correlation of amalgamated turbidite (T-L4–T-L5) with single-bed turbidite (T4) may suggest multiple sources of a turbidite event and large heterogeneity of turbidite deposition within a small distance. As suggested by these turbidite correlations between the two cores, disturbance and/or sediment loss at the core top during piston corer penetration and core recovery is/are small in core PC08. Ikehara et al. (2020) identified frequent turbidite deposition (26 turbidites/2300 years) in core PC08. Hence, the studied small basin at the northern MST might record past large earthquakes with PGAs of $> \sim 0.6$ g near the coring site if the geotechnical and compaction states of surface sediments over the past ~ 100 years have remained the same in the past. The turbidite frequency in core PC08 is higher than those

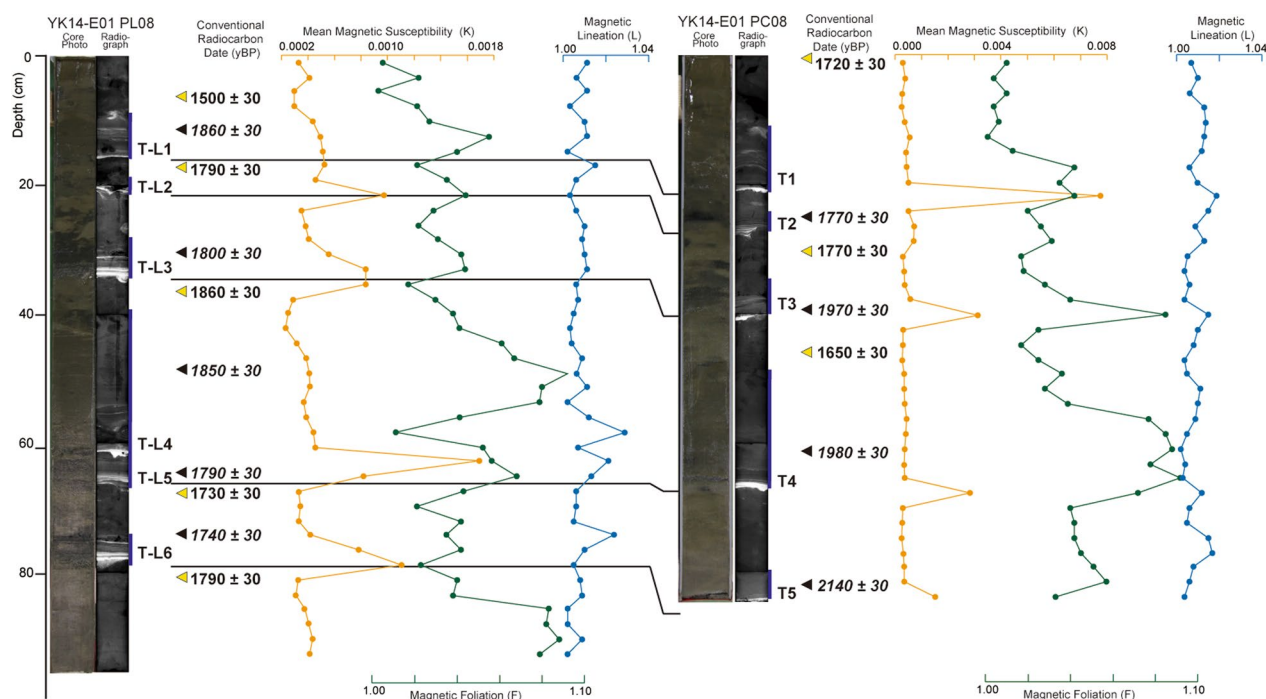


Fig. 4 Correlation of turbidites in core YK14-E01 PL08 with turbidites in the upper part of core YK14-E01 PC08

in two cores at the central MST at $\sim N 39^\circ$ reported by Usami et al. (2018) (~ 12 turbidites/4000 years), although the threshold of PGA (0.4–0.5 g) needed to form earthquake-induced turbidites at the central MST is smaller than that at the northern MST ($> \sim 0.6$ g). The origin of this spatial difference in the PGA threshold for earthquake-induced turbidite deposition along the landward slope of the MST is unclear. The grain size and composition of MST deposits do not change along the MST remarkably. Although the differences in thickness and sedimentation rate of the slope sediments are possible factors, no detailed information about such differences has been obtained. The existence of three types of large ($> Mw \sim 8$) earthquakes in the northern Japan Trench likely contributes to the higher frequency of turbidites in the northern MST ($\sim N 40^\circ$) than in the central MST ($\sim N 39^\circ$). The first type is the interplate earthquakes in the northernmost part of the Japan Trench, such as the 1968 CE Tokachi-oki earthquake. Nagai et al. (2001) suggested that the rupture of a single asperity can produce an M7-class earthquake, such as the 1994 CE Sanriku-oki earthquake, whereas the rupture of multiple asperities can cause M8-class earthquakes, such as the 1968 CE earthquake. The second type is tsunami earthquakes near the trench axis, such as the 1896 CE Meiji–Sanriku earthquake. The third is outer-rise earthquakes caused by the normal faulting of the subducting Pacific Plate, such as the 1933 CE Showa–Sanriku earthquake. There are no clear criteria for distinguishing these types of large earthquakes in marine turbidite records. Deep-sea turbidite deposition caused by a large earthquake occurred all around the rupture area (e.g., the 1993 CE Hokkaido–Nansei-oki earthquake (Ikehara and Usami 2007) and the 2004 CE Sumatra earthquake (Patton et al. 2015)); the spatial distribution of event deposits by each earthquake may be useful for differentiating and characterizing these types. Another possibility of the higher frequency of turbidites in the northern MST is the increase in the PGA threshold in the last few hundred years. If the PGA threshold in the past was smaller than expected, large earthquakes of < 0.6 g could form turbidites in the MST basin. However, no evidence of this possibility exists. It is important to accumulate the results of analysis of more sediment cores along the entire MST for understanding the spatiotemporal variability of the PGA threshold and its controlling factors.

4 Conclusions

To understand how a large PGA is necessary for earthquake-induced surface-sediment remobilization and turbidite deposition, we determined the ages of turbidites in a surface-sediment core PL08 recovered from the northern part of the MST along the inner slope of

the Japan Trench. Small offsets in radiocarbon ages and excess ^{210}Pb activities between turbidite and hemipelagic muds suggest that surface-sediment remobilization may be a major mechanism of turbidite deposition. ^{137}Cs and excess ^{210}Pb chronologies indicate that the three uppermost turbidites in core PL08 are correlated with three large historical earthquakes along the northern Japan Trench: the 1968 CE Tokachi-oki ($Mw 8.2$), 1933 CE Showa–Sanriku ($Mw 8.4$), and 1896 CE Meiji–Sanriku ($Mw \sim 8.1$) earthquakes. We calculate PGAs for large recent and historical earthquakes along the northern Japan Trench using an empirical attenuation relation commonly used in Japan and derived from records of ground motion on land and find that a PGA of ~ 0.6 g is necessary for turbidite deposition in this MST basin. In the MST basins off central Sanriku, turbidites can be deposited by much smaller PGAs (0.4–0.5 g; Usami et al. 2018). Therefore, the PGA threshold for turbidite deposition in the MST basins is spatially variable. This variability should be more thoroughly examined when considering paleoseismic history. The occurrence of three types of large M8-class earthquakes in the northern Japan Trench may contribute to a higher frequency of turbidites in the northern part of the MST ($\sim N 40^\circ$) than in the central part ($\sim N 39^\circ$).

Abbreviations

CE	Common era
MST	Mid-slope terrace
PGA	Peak ground acceleration
IAEA	International Atomic Energy Association

Supplementary Information

The online version contains supplementary material available at <https://doi.org/10.1186/s40645-023-00540-8>.

Additional file 1. Table S1 Magnetic parameters of core YK14-E01 PL08 and the uppermost section (sec. 2) of core YK14-E01 PC08.

Acknowledgements

We express our gratitude to the captain, officers, crews, and marine technicians of the R/V Yokosuka YK14-E-01 cruise for their kind help to collect the core. We thank Dr J.N. Proust and an anonymous reviewer for their constructive comments on the early version of this manuscript as well as Enago for the English language review.

Author contributions

KI and TK projected the study and the survey cruise. KI and KU conducted sedimentological analysis. TK performed magnetic measurements. KI drafted the manuscript. All authors contributed to the data acquisitions and have read and approved the final manuscript.

Funding

This study was supported by JSPS KAKENHI Grant No. 19H05596 and by the MEXT research projects “Geophysical and Geological Studies of Earthquakes and Tsunamis for off-Tohoku District, Japan” and “Research Project for Compound Disaster Mitigation on the Great Earthquakes and Tsunamis around the Nankai Trough Region.”

Availability of data and material

Please contact the corresponding author for data request.

Declarations**Competing interests**

The authors declare that they have no competing interest.

Received: 24 August 2022 Accepted: 16 February 2023

Published: 27 February 2023

References

- Abdeldayam AL, Ikehara K, Yamazaki T (2004) Flow path of the 1993 Hokkaido-Nansei-oki earthquake seismoturbidite, southern margin of the Japan sea north basin, inferred from anisotropy of magnetic susceptibility. *Geophys J Int* 157:15–24
- Adams J (1990) Paleoseismicity of the Cascadia subduction zone: evidence from turbidites off the Oregon-Washington margin. *Tectonics* 9:569–583
- Arai K, Naruse H, Miura R, Kawamura K, Hino R, Ito Y, Inazu D, Yokokawa M, Izumi N, Murayama M, Kasaya T (2013) Tsunami-generated turbidity current of the 2011 Tohoku-Oki earthquake. *Geology* 41:1195–1198. <https://doi.org/10.1130/G347771>
- Balsley JR, Buddington AF (1960) Magnetic susceptibility anisotropy and fabric of some Adirondack granites and orthogneisses. *Am J Sci* 258:6–20
- Bao R, Strasser M, McNichol AP, Haghpor N, McIntyre C, Wefer G, Eglinton TI (2018) Tectonically-triggered sediment and carbon export to the Hadal zone. *Nat Commun* 9:121. <https://doi.org/10.1038/s41467-017-02504-1>
- Beck C (2009) Late Quaternary lacustrine paleo-seismic archives in north-western Alps: examples of earthquake-origin assessment of sedimentary disturbances. *Earth-Sci Rev* 96:327–344
- Campos C, Beck C, Crouzet C, Demory F, Van Welden A, Eris K (2013) Deciphering hemipelagites from homogenites through anisotropy of magnetic susceptibility. Paleoseismic implications (Sea of Marmara and Gulf of Corinth). *Sed Geol* 292:1–14
- Cundy AB, Croudace IW (1995) Physical and chemical associations of radionuclides and trace metals in estuarine sediments: an example from Poole Harbour, Southern England. *J Env Radioact* 29:191–211. [https://doi.org/10.1016/0265-931X\(95\)00031-5](https://doi.org/10.1016/0265-931X(95)00031-5)
- Dan G, Sultan N, Savoye B, Deverchere J, Yelles K (2009) Quantifying the role of sandy-silty sediments in generating slope failures during earthquakes: example from the Algerian margin. *Int J Earth Sci* 98:769–789
- DeMets C, Gordon RG, Argus DF (2010) Geologically current plate motions. *Geophys J Int* 181:1–80
- Fukushima Y, Tanaka T (1990) A new attenuation relation for peak horizontal acceleration of strong earthquake ground motion in Japan. *Bull Seismol Soc Am* 80:757–783
- Furumura T, Kennett BLN (2005) Subduction zone guided waves and the heterogeneity structure of the subducted plate: intensity anomalies in northern Japan. *J Geophys Res* 110:B10302. <https://doi.org/10.1029/2004JB003486>
- Goldfinger C, Morey AE, Has Nelson C, Gutierrez-Pastor J, Johnson JE, Karabanov E, Chaytor J, Eriksson A, Party SS (2007) Rupture lengths and temporal history of significant earthquakes on the offshore and north coast segments of the Northern San Andreas fault based on turbidite stratigraphy. *Earth Planet Sci Lett* 254:9–27
- Goldfinger C, Hans Nelson C, Morey AE, Johnson JE, Patton JR, Karabanov E, Gutierrez-Pastor J, Eriksson AT, Gracia E, Dunhill G, Enkin RJ, Dallimore A, Vallier T (2012) Turbidite event history—methods and implications for Holocene paleoseismicity of the Cascadia subduction zone. USGS Prof Paper, 1661-F, US Geol Surv, Reston
- Headquarters for Earthquake Research Promotion (2019) Evaluations of occurrence potentials of subduction-zone earthquakes along the Japan Trench. https://www.jishin.go.jp/main/chousa/kaikou_pdf/japan_trench.pdf. Accessed 9 July 2022
- Heezen BC, Ewing M (1952) Turbidity currents and submarine slumps, and the 1929 Grand Banks earthquake. *Am J Sci* 250:849–873
- Heezen BC, Ericson DB, Ewing M (1954) Further evidence for a turbidity current following the 1929 Grand Banks earthquake. *Deep-Sea Res* 1:193–202
- Hirose K, Aoyama M, Katsuragi Y, Sugimura Y (1987) Annual deposition of Sr-90, Cs-137 and Pu-239, 240 from the 1961–1980 nuclear explosions: a simple model. *J Met Soc Jpn* 65:259–277
- Hirose K, Igarashi Y, Aoyama M (2008) Analysis of the 50-year records of the atmospheric deposition of long-lived radionuclides in Japan. *Appl Radiat Isot* 66:1675–1678
- Hrouda F (1982) Magnetic anisotropy of rocks and its application in geology and geophysics. *Geophys Surv* 5:37–82
- Igarashi Y, Otsuji-Hatori M, Hirose K (1996) Recent deposition of ⁹⁰Sr and ¹³⁷Cs observed in Tsukuba. *J Environ Radioact* 31:157–169
- Ikehara K, Usami K (2007) Sedimentary processes of deep-sea turbidites caused by the 1993 Hokkaido-nansei-oki earthquake. *Quat Res (Daiyonki-kenkyu)* 46:477–490 ((in Japanese with Eng abstract))
- Ikehara K, Ashi J, Machiyama H, Shirai M (2012) Submarine slope response to earthquake shaking within western Sagami Bay, central Japan. In: Yamada Y et al (eds) *Submarine mass movements and their consequences, advances in natural and technological hazard research*, vol 31. Springer, Dordrecht, pp 539–547
- Ikehara K, Kanamatsu T, Nagahashi Y, Strasser M, Fink H, Usami K, Irino T, Wefer G (2016) Documenting large earthquakes similar to the 2011 Tohoku-oki earthquake from sediments deposited in the Japan Trench over the past 1500 years. *Earth Planet Sci Lett* 445:48–56. <https://doi.org/10.1016/j.epsl.2016.04.009>
- Ikehara K, Usami K, Kanamatsu T (2020) Repeated occurrence of surface-sediment remobilization along the landward slope of the Japan Trench by great earthquakes. *Earth Planet Space* 72:114. <https://doi.org/10.1186/s40623-020-01241-y>
- Ikehara K, Usami K, Irino T, Omura A, Jenkins RG, Ashi J (2021) Characteristics and distribution of the event deposits induced by the 2011 Tohoku-oki earthquake and tsunami offshore of Sanriku and Sendai, Japan. *Sed Geol* 411:105791. <https://doi.org/10.1016/j.sedgeo.2020.105791>
- Iwase R, Momma H, Kawaguchi K, Fujiwara N, Suzuki S, Mitsuzawa K (1997) Turbidity currents on the deep seafloor triggered by the earthquake swarm in the east off Izu Peninsula in March 1997—observation by the long-term deep seafloor observatory off Hatsushima Island in Sagami Bay. *JAMSTEC J Deep Sea Res* 13:433–442 ((in Japanese with Eng abstract))
- Kanai Y (2000) A study on lead-210 dating. Chikyugakagu (geochemistry) 34:23–39 ((in Japanese with Eng abstract))
- Kanamori H (1971) Seismological evidence for a lithospheric normal faulting—The Sanriku earthquake of 1933. *Phys Earth Planet Interior* 4:289–300
- Kase Y, Sato M, Nishida N, Ito M, Mukti MM, Ikehara K, Takizawa S (2016) The use of microstructures for discriminating turbiditic and hemipelagic muds and mudstones. *Sedimentology* 63:2066–2086
- Kato Y, Kitazato H, Shimanaga M, Nakatsuka T, Shirayama Y, Masuzawa T (2003) ²¹⁰Pb and ¹³⁷Cs in sediments from Sagami Bay, Japan: sedimentation rates and inventories. *Prog Oceanog* 57:77–95
- Kitto ME (1991) Determination of photon self-absorption corrections for soil samples. *Int J Radiat Appl Instrum A* 42:835–839
- Larson RA, Brooks GR, Schwing PT, Holmes CW, Carter SR, Hollander DJ (2018) High-resolution investigation of event driven sedimentation: Northeastern Gulf of Mexico. *Anthropocene* 24:40–50
- Lay T (2018) A review of the rupture characteristics of the 2011 Tohoku-oki Mw 9.1 earthquake. *Tectonophysics* 733:4–36
- Lee H, Locat J, Dartnell P, Israel K, Wong F (1999) Regional variability of slope stability: application to the Eel margin, California. *Mar Geol* 154:305–321
- Lykousis V, Roussakis G, Alexandri M, Pavlakis P, Papoulia I (2002) Sliding and regional slope stability in active margins: North Aegean Trough (Mediterranean). *Mar Geol* 186:281–298
- Mann U, Müller G (1980) Composition of sediments of the Japan Trench transect, legs 56 and 57, deep sea drilling project. *Init Rep DSDP* 56(57):939–977
- McHugh CM, Kanamatsu T, Seeber L, Bopp R, Cormier M-H, Usami K (2016) Remobilization of surficial slope sediment triggered by the A.D. 2011 Mw9 Tohoku-Oki earthquake and tsunami along the Japan Trench. *Geology* 44:391–394. <https://doi.org/10.1130/g37650.1>
- Moernaut J, Van Daele M, Heirman K, Fontijn K, Strasser M, Pino M, Urrutia R, De Batist M (2014) Lacustrine turbidites as a tool for quantitative earthquake reconstruction: new evidence for a variable rupture model

- in South Central Chile. *J Geophys Res Solid Earth* 119:1607–1633. <https://doi.org/10.1002/2013JB010738>
- Moernaut J, Van Daele M, Strasser M, Clare MA, Heirman K, Viel M, Cardenas J, Kilian R, de Guevara BL, Pino M, Urrutia R, De Batist M (2017) Lacustrine turbidites produced by surficial slope sediment remobilization: a mechanism for continuous and sensitive turbidite paleoseismic records. *Mar Geol* 384:159–176. <https://doi.org/10.1016/j.margeo.2015.10.009>
- Molenaar A, Moernaut J, Wiemer G, Dubois N, Strasser M (2019) Earthquake impact on active margin: tracing surficial remobilization and seismic strengthening in a slope sedimentary sequence. *Geophys Res Lett* 46:6015–6023. <https://doi.org/10.1029/2019GL082350>
- Molenaar A, Van Daele M, Vandorpe T, Degenhart G, De Batist M, Urrutia R, Pino M, Strasser M, Moernaut J (2021) What controls the remobilization and deformation of surficial sediment by seismic shaking? Linking lacustrine slope stratigraphy to great earthquakes in South-Central Chile. *Sedimentology* 68:2365–2396. <https://doi.org/10.1111/SED.12856>
- Nagai R, Kikuchi M, Yamanaka Y (2001) Comparative study on the source processes of recurrent large earthquakes in Sanriku-oki region: the 1968 Tokachi-oki Earthquake and the 1994 Sanriku-oki Earthquake. *Zisin* 2(54):267–280 ((in Japanese with Eng abstract))
- Nagata T (1961) Rock magnetism, 2nd edn. Maruzen, Tokyo, p 350
- Noda A, Tuzino T, Kanai Y, Furukawa R, Uchida J-I (2008) Paleoseismicity along the southern Kuril Trench deduced from submarine-fan turbidites. *Mar Geol* 254:73–90
- Oguri K, Kawamura K, Sakaguchi A, Toyofuku T, Kasaya T, Murayama M, Fujikura K, Glud RN, Kitazato H (2013) Hadal disturbance in the Japan Trench induced by the 2011 Tohoku-Oki earthquake. *Sci Rep* 3:1915. <https://doi.org/10.1038/srep01915>
- Okutsu N, Ashi J, Yamaguchi A, Irino T, Ikehara K, Kanamatsu T, Suganuma Y, Murayama M (2019) Evidence for surface sediment remobilization by earthquakes in the Nankai forearc region from sedimentary records. In: Lintern DG, Mosher DC, Moscardelli LG, Bobrowsky PT, Campbell C, Chaytor, J, Clague J, Georgiopoulou P, Lajeunesse P, Normandeau A, Piper D, Scherwath M, Stacey C, Turmel D (eds.) Submarine mass movements and their consequences: assessing geohazards, environmental implications and economic significance of subaqueous landslides. *Spec Publ* no. 477, Geol Soc London, pp. 37–45. <https://doi.org/10.1144/SP477.22>
- Patton JR, Goldfinger C, Morey AE, Ikehara K, Romsos C, Stoner J, Djadjadiharja Y, Ardhyasturi SU, Gaffer EZ, Viscaino A (2015) A 6600 year earthquake history in the region of the 2004 Sumatra-Andaman subduction zone earthquake. *Geosphere* 11:1–62
- Petersen J, Wilhelm B, Revel M, Rolland Y, Crouzet C, Arnaud F, Brisset E, Chaumillon E, Magand O (2014) Sediments of Lake Vens (SW European Alps, France) record large-magnitude earthquake events. *J Paleolimnol* 51:343–355
- Pickering KT, Hiscott RN (2015) Deep marine systems: processes, deposits, environments, tectonics and sedimentation. AGU and Wiley, Chichester, p 657p
- Piper DJW, Cochonat P, Morrison ML (1999) The sequence of events around the epicentre of the 1929 Grand Banks earthquake: initiation of debris flows and turbidity current inferred from sidescan sonar. *Sedimentology* 46:79–97
- Pouderoux H, Proust J-N, Lamarche G (2014) Submarine paleoseismology of the northern Hikurangi subduction margin of New Zealand as deduced from Turbidite record since 16 ka. *Quat Sci Rev* 84:116–131
- Saino T, Shang S, Mino Y, Suzuki K, Nomura H, Saito S, Miyake H, Masuzawa T, Harada K (1998) Short term variability of particle fluxes and its relation to variability in sea surface temperature and Chlorophyll a field detected by ocean color and temperature scanner (OCTS) off Sanriku, Northwestern North Pacific in the spring of 1977. *J Oceanogr* 54:583–592
- Satake K (2015) Geological and historical evidence of irregular recurrent earthquakes in Japan. *Phil Trans R Soc A* 373:20140375. <https://doi.org/10.1098/rsta.2014.0375>
- Satake K, Fujii Y, Yamaki S (2017) Different depths of near-trench slips of the 1896 Sanriku and 2011 Tohoku earthquakes. *Geosci Lett* 4:33. <https://doi.org/10.1186/s40562-017-0099-y>
- Schwestermann T, Eglinton TI, Haghipour N, McNichol AP, Ikehara K, Strasser M (2021) Event-dominated transport, provenance, and burial of organic carbon in the Japan Trench. *Earth Planet Sci Lett* 563:116870. <https://doi.org/10.1016/j.epsl.2021.116870>
- Si H, Midorikawa S (1999) New attenuation relationships for peak ground acceleration and velocity considering effects of fault type and site condition. *J Struct Constr Eng* 64(523):63–70. https://doi.org/10.3130/aajs.64.63_2. ((in Japanese with Eng abstract))
- Si H, Koketsu K, Miyake H (2016) Attenuation characteristics of strong ground motion from megathrust earthquakes in subduction zone –on the pass effects. *J Jpn Assoc Earthq Eng* 16:96–105 ((in Japanese with Eng abstract))
- Stacey FD, Joplin G, Lindsay J (1960) Magnetic anisotropy and fabric of some foliated rocks from S.E. Australia. *Geofis Pura Appl* 47:30–40
- Stow DAV, Shanmugam G (1980) Sequence of structures in fine-grained turbidites: comparison of recent deep-sea and ancient flysch sediments. *Sed Geol* 25:23–42
- Strasser M, Stegmann S, Bussmann F, Anselmetti FS, Rick B, Kopf A (2007) Quantifying subaqueous slope stability during seismic shaking: Lake Licerne as model for ocean margins. *Mar Geol* 240:77–97
- Tajima F, Mori J, Kennett BLN (2013) A review of the 2011 Tohoku-Oki earthquake (Mw 9.0): large-scale rupture across heterogeneous plate coupling. *Tectonophysics* 586:15–34
- Tarling DH, Hrouda F (1993) The magnetic anisotropy of rocks. Chapman and Hall, London, p 217
- Toda S (2016) Crustal earthquakes. In: Moreno T, Wallis S, Kojima T, Gibbons W (eds) The geology of Japan. Geol Soc, London, pp 371–408
- Tsuru T, Park J-O, Miura S, Kodaira S, Kido Y, Hayashi T (2002) Along-arc structural variation of the plate boundary at the Japan Trench margin: implication of interpolate coupling. *J Geophys Res* 107(B12):2357. <https://doi.org/10.1029/2001JB001664>
- Usami K, Ikehara K, Kanamatsu T, McHugh CM (2018) Supercycle in great earthquake recurrence along the Japan Trench over the last 4000 years. *Geosci Lett* 5:11. <https://doi.org/10.1186/s40562-018-0110-2>
- von Huene R, Culotta R (1989) Tectonic erosion at the front of the Japan Trench convergent margin. *Tectonophysics* 160:75–90
- von Huene R, Langseth M, Nasu N, Okada H (1980) summary, Japan Trench transect. *Init Rep DSDP* 56(57):473–488
- Yoshida Y, Ueno H, Muto D, Aoki S (2011) Source process of the 2011 off the Pacific coast of Tohoku Earthquake with the combination of teleseismic and strong motion data. *Earth Planet Space* 63:565–569
- Zhao JX, Dowrick DJ, McVerry GH (1997) Attenuation of peak ground accelerations in New Zealand earthquakes. *Bull N Z Soc Earthq Eng* 30:133–158

Publisher's Note

Springer Nature remains neutral with regard to jurisdictional claims in published maps and institutional affiliations.

Submit your manuscript to a SpringerOpen[®] journal and benefit from:

- Convenient online submission
- Rigorous peer review
- Open access: articles freely available online
- High visibility within the field
- Retaining the copyright to your article

Submit your next manuscript at ► [springeropen.com](https://www.springeropen.com)